The Astrophysical Journal, 889:69 (8pp), 2020 January 20 https://doi.org/10.3847/1538-4357/ab5c20

Filling the Magnetospheres of Weak Pulsars

Alexander Y. Chen[1], Fábio Cruz[2], and Anatoly Spitkovsky[1]
[1] Department of Astrophysical Sciences, Princeton University, Princeton, NJ 08544, USA; alexc@astro.princeton.edu
[2] GoLP/Instituto de Plasmas e Fusão Nuclear, Instituto Superior Técnico, Universidade de Lisboa, 1049-001 Lisbon, Portugal
Received 2019 October 31; accepted 2019 November 25; published 2020 January 27

Abstract

Recent advances in numerical algorithms and computational power have enabled first-principles simulations of pulsar magnetospheres using particle-in-cell techniques. These ab initio simulations seem to indicate that pair creation through photon–photon collision at the light cylinder is required to sustain the pulsar engine. However, for many rotation-powered pulsars, pair creation operates effectively only near the stellar surface where magnetic field is high. How these "weak pulsars" fill their magnetospheres without efficient photon–photon pair conversion in the outer magnetosphere is still an open question. In this paper, we present a range of self-consistent solutions to the pulsar magnetosphere that do not require pair production near the light cylinder. When pair production is very efficient near the star, the pulsar magnetosphere converges to previously reported solutions. However, in the intermediate regime, where pair supply is barely enough to sustain the magnetospheric current, we observe a time-dependent solution with a quasi-period about half of the rotation period. This new quasi-periodic solution may explain the observed pulsar death line without invoking multipolar components near the star, and can potentially explain the core versus conal emission patterns observed in pulsar radio signals.

Unified Astronomy Thesaurus concepts: Plasma astrophysics (1261); Rotation powered pulsars (1408); Magnetic fields (994); Neutron stars (1108)

1. Introduction

Over the past few years, significant progress toward understanding how pulsars work has been made with the help of direct particle-in-cell (PIC) simulations. With enough pair supply, the pulsar magnetosphere is well described by the force-free solution, forming a Y-point near the light cylinder, which connects an equatorial current sheet and two curved current sheets along the separatrix between closed and open field lines. Particles are accelerated along these current sheets, and it is possible to construct the observed gamma-ray light curves from these first principle simulations (Cerutti et al. 2016; Philippov & Spitkovsky 2018). It was also shown that general relativistic effects, although small, are important to allow certain regions of the polar cap to create pairs, enabling radio emission (Philippov et al. 2015a).

The electrodynamics of the pulsar magnetosphere is predicated on sufficient supply of plasma, but less sensitive to where the plasma is produced. Directly injecting particles everywhere in the magnetosphere (e.g., Philippov & Spitkovsky 2014), injecting pairs artificially from the surface (e.g., Cerutti et al. 2015; Brambilla et al. 2018), or self-consistent pair creation (e.g., Chen & Beloborodov 2014, hereafter CB14; Philippov et al. 2015b) all seem to give a global picture similar to force-free, as long as the pair creation rate is large enough.

However, the location of pair production becomes important when pair supply becomes low and deviation from force-free becomes more evident. CB14 pointed out that there are two classes of pulsars, and they may have qualitatively different magnetospheric structures. Type I pulsars have significant optical depth to γ–γ pair production near the light cylinder. These are mostly young and rapidly rotating pulsars like the Crab, and include most known gamma-ray pulsars. They tend to form a force-free magnetosphere with Y-shaped current sheets, launching a pulsar wind of high multiplicity pair plasma. Type II pulsars are those that do not have enough opacity to γ–γ collision, and their main accessible channel to produce $e^{\pm}$ pairs is through magnetic conversion. Since this process requires very high magnetic fields, comparable to the quantum critical field B_Q, it is only operational near the stellar surface. These pulsars make up a significant fraction of known radio pulsars, and understanding how they operate is an important problem. There are different conclusions in the literature. CB14 concluded that type II pulsars require misalignment to be active, otherwise they settle to a charge-separated solution similar to an "electrosphere" (e.g., Krause-Polstorff & Michel 1985). Cerutti et al. (2015) were able to find an intermediate aligned rotator solution that has a thick equatorial current sheet and less spindown power than the force-free solution, using a low rate of pair injection from the surface of the star. These type II pulsars were also called "weak pulsars" by Gruzinov (2015), who obtained a solution that has large vacuum gaps and can convert up to 50% of the spindown power to radiation (Gruzinov 2012).

In this paper, we investigate how pulsars of type II, or "weak pulsars" (we will use these two terms interchangeably), support their magnetospheres and produce observable radiation. In Section 2 we discuss the microphysics of polar cap pair creation and how it maps to PIC simulations, in order to motivate the parameter regimes used in our runs. In Section 3 we discuss our numerical setup and several implementation choices, and in Section 4 we present the solutions we find in different parameter regimes, analyzing them in detail. In Section 5 we discuss the relevance of the models found in this paper in the context of existing pulsar theory and phenomenology. Finally in Section 6 we conclude with a discussion on the limitations of this paper and possible future directions.

2. Theoretical Motivation

We consider only magnetic conversion of γ-ray photons into pairs since it is the dominant pair production mechanism in the

magnetospheres of weak pulsars. The cross section of this process depends exponentially on the ratio between local magnetic field B and the quantum critical field, B/B_Q, where $B_Q = m_e^2 c^3/\hbar e \approx 4.4 \times 10^{13}$ G (see, e.g., Erber 1966). When $B \ll B_Q$ this process is exponentially suppressed, which means it can only operate very close to the star where $B/B_Q \gtrsim 0.1$. It is possible to model this as a sharp cutoff radius $R_{\rm cut}$, outside of which pair creation is not allowed. Depending on the local B field, $R_{\rm cut}$ is typically several stellar radii, R_*.

There are three energy scales governing the pair creation process near the polar caps of pulsars. The maximum potential drop across a pulsar polar cap can be estimated as $\Phi_{\rm pc} \sim \mu_B \Omega^2/c^2$, (e.g., Ruderman & Sutherland 1975), which translates to a maximum Lorentz factor achievable by particles,

$$\gamma_{\rm pc} = \frac{e\Phi_{\rm pc}}{m_e c^2} \sim 1.2 \times 10^7 B_{12} P^{-2}, \quad (1)$$

assuming $B_0 = B_{12} \times 10^{12}$ G at the pole, and period P is measured in seconds. $\Phi_{\rm pc}$ is the maximum potential drop across the polar cap, but in reality the polar cap gap may not reach this potential drop, as the gap will start to be screened as soon as pairs are produced. The actual polar cap voltage is expected to be lower and regulated by pair creation activity.

The second energy scale is the energy of accelerated particles that are capable of emitting pair-producing photons. We loosely call this pair-creating Lorentz factor $\gamma_{\rm thr}$. In classic pulsar theory, high energy gamma-ray photons are produced through the curvature radiation of primary particles, and the typical photon energy is $\hbar\omega_c = 3\gamma^3\hbar c/2\rho_c$, where ρ_c is the radius of curvature of the particle trajectory. The optical depth of the curvature photons depends on the quantum parameter $\chi \sim \epsilon_\gamma b \sin\psi$, where ϵ_γ is the photon energy in units of $m_e c^2$, $b = B/B_Q$, and ψ is the angle between the photon momentum and local B field. When the photon is emitted, the angle ψ is negligible due to strong Lorentz boost along the parallel direction, and ψ builds up nearly linearly with distance traveled by the photon. Conversion of the photon to pairs happens roughly when $\chi \sim 0.1$ (Timokhin & Harding 2019). If one requires the photon to convert within 1 R_* from the surface (before the field strength drops too low), then one can estimate the pair creation threshold to be:

$$\gamma_{\rm thr} \sim \left(\frac{B_Q \rho_c^2 m_e c}{15 B_0 R_* \hbar}\right)^{1/3} \sim 8.6 \times 10^6 B_{12}^{-1/3} P^{1/3}, \quad (2)$$

assuming dipole field and curvature radius along the last closed field line. Depending on the actual B field strength near the surface and field line geometry, this threshold can vary significantly. For example, a multipolar component near the polar cap can vastly reduce the curvature radius of the field lines, lowering the threshold by orders of magnitude. The ratio $\gamma_{\rm pc}/\gamma_{\rm thr}$ determines whether pair creation is efficient, and large values of this ratio indicate the ease of converting the voltage drop to high pair multiplicity. Conversely, values of $\gamma_{\rm pc}/\gamma_{\rm thr}$ that approach unity indicate inefficient pair production, which is associated with the cessation of pulsar activity, and corresponds to the pulsar "death line" in the P–$\dot{P}$ plane. We will continue the discussion of the pulsar death line in Section 5.

The third energy scale is the typical energy of secondary pairs γ_s. The energies of the curvature photons emitted by the primary particles near $\gamma_{\rm thr}$ are much lower than the energy of the emitting particle, and will set an energy scale for secondary pairs:

$$\gamma_s \sim \frac{3}{4}\frac{\hbar}{m_e c^2}\frac{\gamma_{\rm thr}^3}{\rho_c} \sim 200 B_{12}^{-1} P^{-1/2}. \quad (3)$$

The ratio $\gamma_{\rm thr}/\gamma_s$ is a major factor in regulating the pair multiplicity from the polar cap cascade, as it determines how many pairs can one primary particle generate.

In general, for pulsars away from the death line, the energy scales should obey the hierarchy: $1 \ll \gamma_s \ll \gamma_{\rm thr} \ll \gamma_{\rm pc}$. In a PIC simulation, especially a global one, this kind of scale separation is typically not achievable, and one has to rescale the energies preserving the ordering of scales. For example, in the Type-II case presented in CB14, $\gamma_{\rm pc} \sim 425$ (referred to as γ_0 in that paper), $\gamma_{\rm thr} \sim 25$, and $\gamma_s \sim 10$. In the global simulations published so far, typically $\gamma_{\rm pc} \lesssim 1000$, with $\gamma_{\rm thr}$ and γ_s similar to CB14. This reduced scale separation has two effects. First, it severely limits the multiplicity of any pair cascade triggered in the magnetosphere from energetics alone, as a primary particle with Lorentz factor $\gamma_{\rm thr}$ can only convert its energy to one or two $e^\pm$ pairs with γ_s, whereas in reality it would be $\gtrsim 10^3$. It also places the simulated pulsars dangerously close to the death line, as the ratio $\gamma_{\rm pc}/\gamma_{\rm thr}$ is merely of order $\sim$10.

In this paper, we approach this issue by pushing up the ratio $\gamma_{\rm pc}/\gamma_{\rm thr}$, in order to better approximate a pulsar that is far from the death line but still not energetic enough to produce pairs near the light cylinder. This is also a regime that is easier to simulate since when $\gamma_{\rm pc}/\gamma_{\rm thr} \gg 1$, typical curvature photons have relatively short free path in the strong magnetic field, and "on-the-spot" pair creation scheme is applicable. We vary this ratio to study the transition of an active rotation-powered radio pulsar to its death. On the other hand, we keep the ratio $\gamma_{\rm thr}/\gamma_s$ low across the simulations in order to keep the pair multiplicity and total number of particles manageable in our simulations.

3. Simulation Setup

We simulate an aligned rotator whose magnetic axis is parallel to the rotation axis, using the code *Aperture* (Chen 2017). The neutron star is placed at the origin in log-spherical coordinates. We assume axisymmetry and simulate the magnetosphere in the r–θ plane. The simulation domain extends from the stellar surface to about $4R_{\rm LC}$, where $R_{\rm LC}$ is the light cylinder radius. Unless stated otherwise, we use $R_{\rm LC}/R_* = 8$ and allow pair creation up to radius $R_{\rm cut} = 3R_*$. Pair creation happens whenever an electron/positron reaches the Lorentz factor $\gamma_{\rm thr} = 25$ within the pair creation radius, and an $e^\pm$ pair is created instantly at $\gamma_s = 8$. The simulations shown in this paper all have resolution 2048×2048, which translates to about 650 grid points per R_* at the stellar surface.

The star is initially at rest and spins up to the target angular velocity Ω_* over $t_{\rm spin} = 10R_*/c$. We start with a pure dipole magnetic field in vacuum. Particles injected at the surface are assigned a weight $w \propto \sin\theta$, which varies with the volume of the cell where they are injected. This weight carries over to new pairs, and can be understood as the amount of physical particles represented by a given macro-particle in the simulation. We apply the spin as a boundary condition at the stellar surface, $E_\theta = -v_\phi B_r$, where v_ϕ is given by the Lense–Thirring reduced

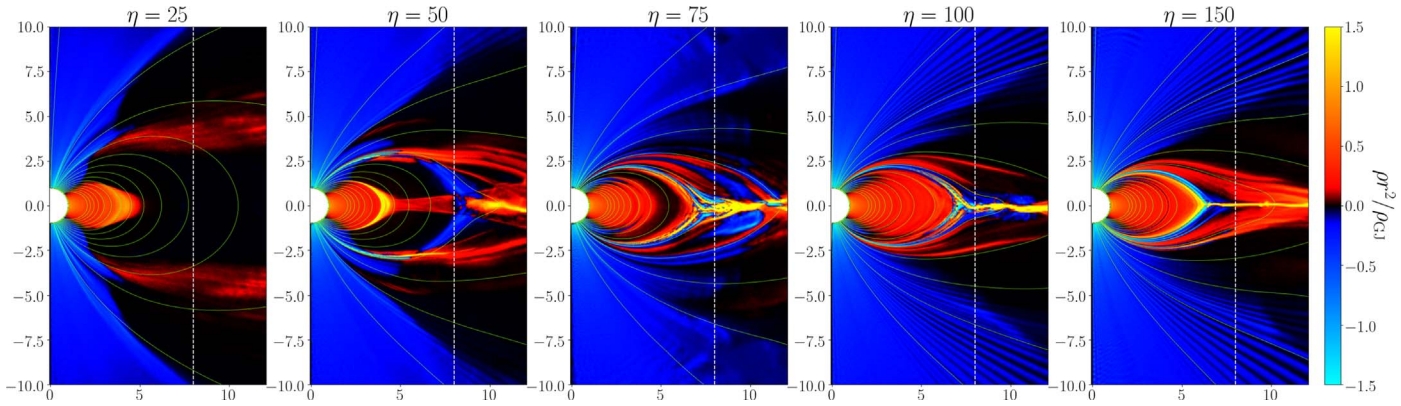

Figure 1. Comparison of five different simulations of different ratios $\eta = \gamma_{pc}/\gamma_{thr}$ at the same snapshot time $t = 90R_*/c$. Plotted in color is the charge density in the magnetosphere, multiplied by a factor of r^2 to better visualize features away from the star. Each case is normalized to its own $\rho_{GJ} = \Omega B_0/2\pi c$. Vertical white dashed line is the light cylinder, and green curves are magnetic field lines.

angular velocity (Philippov et al. 2015b):

$$v_\phi = \frac{(\Omega_* - \omega_{LT}) r \sin\theta}{c\alpha}. \quad (4)$$

We use the compactness parameter $r_s/R_* = 0.5$ for all our runs. General relativity (GR) effects are taken into account in the field equations similarly to what was used by Philippov & Spitkovsky (2018), namely using a dipole background B field for the $\nabla \times B$ term in the E field update equation. This GR correction effectively reduces the background charge density $\rho_{GJ} = \Omega B/2\pi c$ near the polar cap, increasing the ratio the current j and $\rho_{GJ} c$ to above unity, therefore allowing pair production to happen near the pole.

We also include strong synchrotron cooling to reduce the magnetic bottling effect for plasma flowing toward the star. We damp directly the perpendicular momentum $p_\perp$ of electrons and positrons at every timestep, and the strength of this damping is directly proportional to local B field. An electron would typically lose almost all its perpendicular momentum in about 20 timesteps near the stellar surface.

We define the ratio $\eta = \gamma_{pc}/\gamma_{thr}$ and fix Ω and γ_{thr}, while increasing η by increasing B_0, which is the dipolar magnetic field strength at the equator of the star. In the following section, we report the results of this series of numerical experiments.

4. Results

4.1. A Range of Weak Pulsar Solutions

By increasing the ratio η, we see a transition through very different solutions to the weak pulsar magnetosphere. Figure 1 shows a comparison of five runs with increasing η. The case with $\eta = 25$ is very similar to the original Type-II solution reported in CB14. The pulsar settles down to a state with very low spindown power, with a large vacuum gap outside the pair creation radius R_{cut}. There is still a small current escaping the polar cap and along the field line that touches the light cylinder, and some remnant pair creation activity launches positrons into the vacuum gap which supports the return current. However, all field lines remain closed, and the small remnant current is conducted by escaping charges accelerated by the vacuum gap, moving across field lines. On a much longer timescale, we expect the current to gradually decrease as the magnetospheric solution settles down to an electrosphere.

The cases with $\eta = 50$ and $\eta = 75$ are highly variable. Figure 1 is a snapshot of the magnetospheric configuration, but both solutions are actually cyclic, with episodes of pair creation along the return current sheet that launch $e^\pm$ pairs toward the light cylinder. When this quasi-neutral plasma outflows, it screens the electric field up to the Y-point, and forms a charge cloud there. This charge cloud later depletes, with electrons flowing back toward the star along the separatrix, and positrons flowing to infinity in the equatorial current sheet. This case will be discussed in more detail in Section 4.2.

The cases with $\eta = 100$ and $\eta = 150$ are quasi-steady again, with field lines that go through the light cylinder opening up, forming a stable Y-point near the light cylinder and persistent return current sheets. We observe reconnection of the poloidal magnetic flux and plasmoids forming periodically in the equatorial current sheet near the Y-point, similar to the Type I pulsar reported in CB14. Both cases approach the force-free limit with similar polar cap outflow multiplicity.

Figure 2 shows the time evolution of spindown power for the different γ_{pc}/γ_{thr} cases, measured as the integrated Poynting flux from the stellar surface, normalized to the respective force-free spindown $L_0 = \mu^2\Omega^4/c^3$ of each run. The Poynting flux is defined with GR effect taken into account. It can be seen that after a common initial transient, the runs with $\eta = 100$ and $\eta = 150$ settle to a quasi-steady state with almost force-free spindown, whereas the intermediate η runs show quasi-periodic swings in spindown luminosity which are in-phase with the pair creation episodes. The $\eta = 25$ case sees a gradual drop in spindown luminosity, approaching roughly 0.1–0.2 of the force-free spindown. We expect the spindown power to slowly decrease to zero, as the magnetosphere settles down to a state similar to the electrosphere. This was the fate of the weak pulsar proposed in CB14.

Figure 3 shows the radial dependence of the integrated Poynting flux for the different cases. It can be seen that $\eta = 100$ and $\eta = 150$ cases have very little dissipation of the Poynting flux inside the light cylinder, but about 20% of it is dissipated between $r = R_{LC}$ and $2R_{LC}$. The dissipation mainly happens in the equatorial current sheet. This agrees very well quantitatively with the high particle injection case reported by Cerutti et al. (2015). As a result, we expect most of the high energy γ-ray emission for these pulsars to come from outside the light cylinder, in the equatorial current sheet, similar to what was reported by Cerutti et al. (2016) and Philippov & Spitkovsky (2018). The intermediate solutions, however, see a

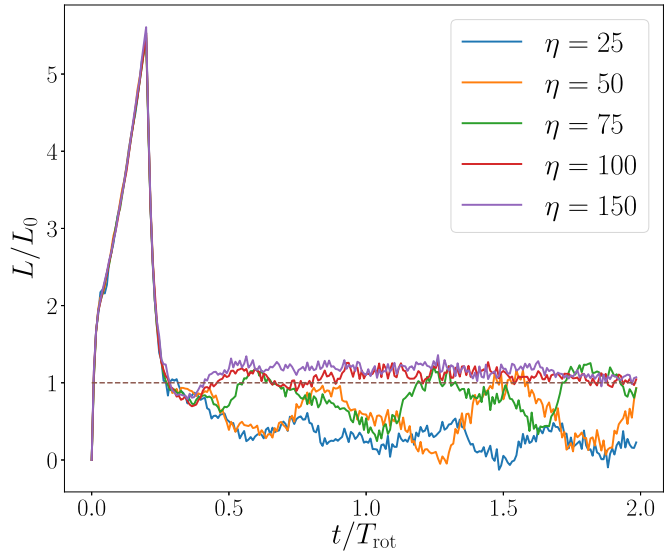

Figure 2. Time evolution of the total Poynting flux from the star for the different parameters, normalized to the force-free spindown power $L_0 = \mu^2\Omega^4/c^3$.

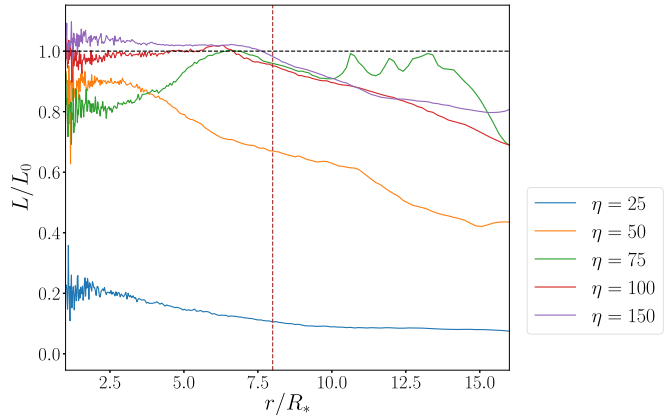

Figure 3. Integrated Poynting flux as a function of radius, for the different cases discussed in the text, all normalized to the force-free spindown $L_0 = \mu^2\Omega^4/c^3$. This snapshot is taken at $t \sim 2T_{\rm rot}$. Vertical dashed line marks the light cylinder.

somewhat higher dissipation inside the light cylinder, up to 10%–20%. This suggests that in these solutions a fraction of the spindown power can in principle be dissipated into particle kinetic energy within the light cylinder, in agreement with the recurrent large vacuum gaps reported in Section 4.2. In Figure 3, the $\eta = 75$ case seems to suggest energy injection near the light cylinder, but it is simply a result of the time-dependent nature of the solution, as the Poynting flux from the star goes through large-amplitude oscillations.

It is also instructive to look at where pairs are created. Figure 4 shows the pair creation sites, with and without GR effect. It can be seen that pairs are only created at the center of the polar cap and along the separatrix current sheet. These are the sites where $j/\rho_{\rm GJ}c$ is either above unity or below zero, which are expected to require pair production to conduct the magnetospheric current (Beloborodov 2008). Without GR effect, there is no polar cap pair creation, in line with what was reported by Philippov et al. (2015a). It is curious, however, that even without GR effect and pair creation at the center of the polar cap, the pulsar is capable of supporting the structure of the magnetosphere with only pairs created along the separatrix current sheet. If we believe that radio emission is associated with high plasma multiplicity at the polar cap, then GR effect is essential for turning on radio emission for many pulsars, especially if their rotation and magnetic axes are nearly aligned. However, it turns out to be not so important for the structure of the magnetosphere, as the magnetospheric current can be conducted simply by extracted electrons flowing at mildly relativistic speeds, which agrees with what was reported by Chen & Beloborodov (2013) and Timokhin & Arons (2013).

Plasma supply is the key factor that differentiates the range of pulsar solutions. One way to quantify this is to define the global pair multiplicity, defined as

$$\mathcal{M} = \frac{\int d\Omega \int_{R_*}^{R_{\rm LC}} e(n_+ + n_-)dr}{\int d\Omega \int_{R_*}^{R_{\rm LC}} |\rho_{\rm GJ}|\, dr}, \tag{5}$$

where $n_\pm$ are electron and positron number densities. This quantity measures how much plasma is produced in excess to the minimum Goldreich-Julian (GJ) charge density. Figure 5 shows the time evolution of this multiplicity for the different runs considered. It can be seen that going from $\eta = 100$ to $\eta = 150$ increases the pair multiplicity during the initial transient, but the system settles down to a similar global multiplicity. The polar cap acceleration potential Φ in these two cases also capped at $\Phi_{\rm thr}$, much less than the theoretical $\Phi_{\rm pc}$, in agreement with the discussion in Section 2. The intermediate cases see oscillations in multiplicity that mirror the time-dependence in the light curves. The fact that the overall global multiplicity is increasing for both cases strongly suggests that these solutions are self-sustaining and should be stable in the long term.

4.2. The Oscillatory Intermediate Solution

The intermediate solution where the magnetospheric structure of the pulsar is highly time-dependent is particularly interesting. Figure 6 shows the time evolution of various magnetospheric quantities over one such cycle. It starts with quasi-neutral plasma outflowing from the pair creation surface at $r \sim 3R_*$ (column 1, electron and positron densities near the separatrix), screening the parallel electric field along the separatrix,[3] momentarily forming the separatrix current sheet and the Y-point outside the light cylinder (columns 2–3, see current and $\boldsymbol{E}\cdot\boldsymbol{B}$). As the parallel electric field becomes screened, pair creation activity is reduced, and the return current can no longer be sustained. At this point the electrons in the outer magnetosphere start to fall back onto the star to conduct the return current (columns 4–5, see electron density). These electrons are accelerated toward the star because $E_\parallel$ is induced again due to insufficient current. They start to create pairs when they reach the pair creation surface at $r \sim 3R_*$ and reignite the pair creation, eventually launching a quasi-neutral outflow again, initiating the next cycle (columns 5–6, electron and positron densities).

[3] The "separatrix," usually denoting the return current sheet formed along the last closed field line, loses the usual meaning here as most field lines remain closed. We simply use this term to denote the strong return current flowing in the vicinity of the usual separatrix.

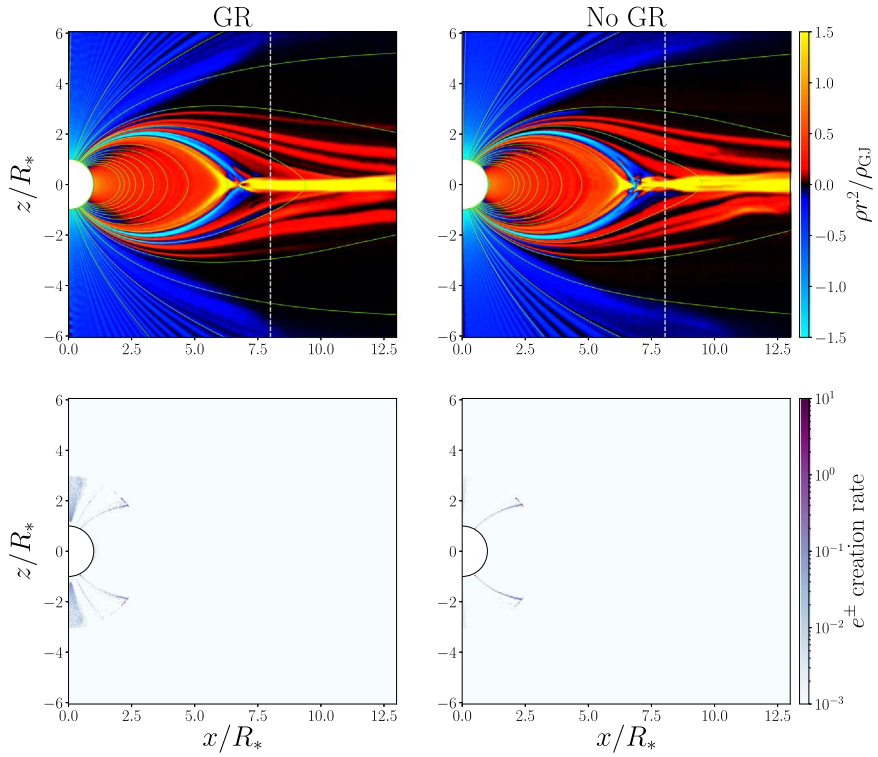

Figure 4. Pair creation sites, with and without GR, in the $\eta = 100$ case. Snapshot is taken at $t \approx 2T_{\rm rot}$. The upper panels show the charge density and magnetic field structure similar to Figure 1, while the lower panels show pair creation rates per cell normalized to arbitrary units around the same time, averaged over $\Delta T = R_*/c$. Pair creation at the center of the polar cap is notably missing in the non-GR simulation, while both have pair creation along the separatrix current sheet. Even without polar cap pair production, the magnetospheric structure remains exactly the same.

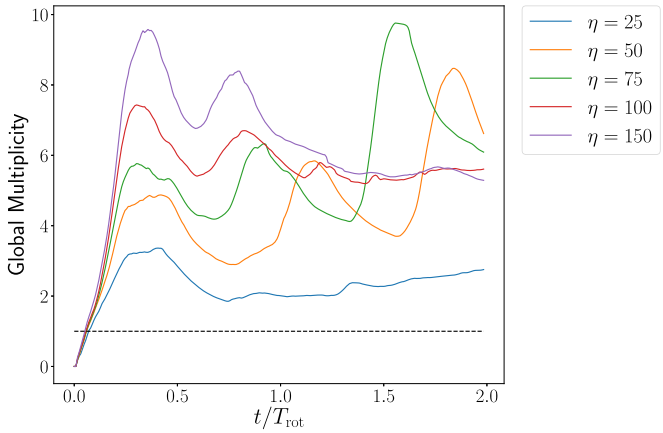

Figure 5. Global multiplicity evolution for the near force-free cases. Black dashed line represents $\mathcal{M} = 1$. The higher η runs have higher multiplicity during the initial transient. The $\eta = 100$ and 150 cases both relax to a similar global multiplicity, while the two intermediate runs show the same kind of quasi-periodic oscillations in the multiplicity. The lowest η run is never able to sustain the same amount of pairs, as expected from the spindown comparison.

Even in the quasi-stationary force-free like solution with $\eta = 100$ or 150, we still observe this cyclic behavior to some degree. The pairs outflowing along the separatrix current sheet tend to form a charge cloud near the Y-point. A stream of electrons is drawn from the Y-point cloud to help support the return current, and these electrons are accelerated on their way toward the star, producing pairs as they come close to the stellar surface. A fraction of these pairs outflow again, carrying stronger return current and screening $E_\parallel$ along the separatrix, thus reducing the acceleration voltage on the returning electrons and suppressing pair creation. The $E_\parallel$ oscillations are much smaller in amplitude than in the intermediate regime, but could potentially contribute to the complex time-dependent behavior we see in pulsar radio emission.

We observe the period of this quasi-cycle to be near half of the rotation period, comparable to the travel time between the star and the light cylinder for relativistic particles along the last closed field line. However, we believe the period can depend on the multiplicity from the pair cascade near $r \sim 3R_*$, since if more pairs outflow during the active phase, more electrons can be stored in the Y-point charge cloud which takes longer to deplete. If this is true, higher multiplicity should translate to a longer duty cycle. In this paper we are unable to perform simulations with much higher multiplicity due to computational constraints, since higher multiplicity requires a finer grid, consumes larger memory, and leads to high local concentration of particles that make simulations difficult. We will defer the study of the multiplicity dependence of the cyclic solution to a future work.

5. Implications of the Time-dependent Weak Pulsar Model

The time-dependent intermediate solution presented in Section 4.2 is a result of $\gamma_{\rm pc}/\gamma_{\rm thr} = 50$, but is more representative of pulsars when the polar cap pair supply is marginally enough to sustain the magnetosphere. The same description is usually applied to pulsars near the death line, as it is conventionally believed that a high plasma multiplicity from pair creation is essential in producing the observed pulsar radio emission. The pulsar death line has been studied in great detail before (e.g., Chen & Ruderman 1993; Zhang et al. 2000; Hibschman & Arons 2001), and most authors conclude that a dipolar magnetic field is not enough to explain the observed

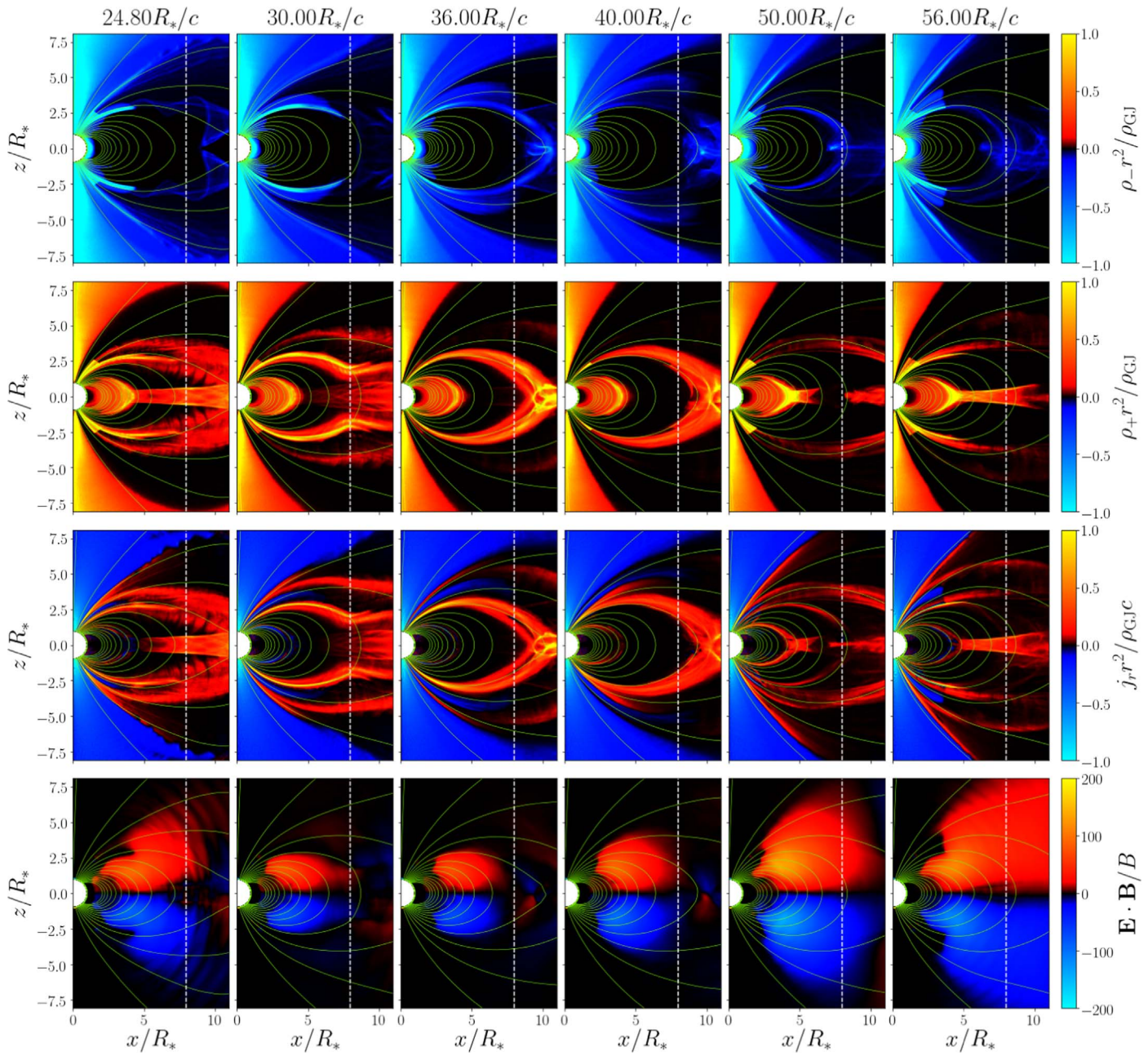

Figure 6. $\eta = 50$ case in detail. From left to right shows evolution in time. The six panels together show a complete cycle. From top to bottom the color plots show (a) electron density $\rho_- r^2$, (b) positron density $\rho_+ r^2$, (c) radial current $j_r r^2$, and (d) $\boldsymbol{E}\cdot\boldsymbol{B}/B$. The charge and current densities are normalized to $\rho_{\rm GJ}$ at the pole, and $\boldsymbol{E}\cdot\boldsymbol{B}$ is in numerical units. White vertical dashed lines mark the light cylinder, and green lines show the magnetic field.

death line. In fact, if the high energy γ rays from curvature radiation are the main pair-creating photons, then the death line computed from polar cap voltage assuming a dipole field configuration can be found by equating $\gamma_{\rm pc}$ to $\gamma_{\rm thr}$ (Equations (1) and (2)), which lies somewhere in the middle of the observed pulsar population (Chen & Ruderman 1993). Usually some non-dipolar configuration is invoked to decrease the radius of curvature of pair-producing field lines, and push the death line down to allow for many observed weak pulsars, regardless of whether curvature radiation or inverse Compton scattering is the main γ ray producing mechanism.

Another seemingly unrelated piece of the puzzle is that isolated rotation-powered radio pulsars fall in two populations. Younger and more energetic pulsars tend to have a clearly defined core radio emission pattern, while the older and less energetic pulsars tend to have a multiple conal emission structure (see, e.g., Rankin 1983). The line separating these two populations is surprisingly close to the naive death line of a dipole polar cap cascade model (see, e.g., Weatherall & Eilek 1997). The details of pair creation mechanism and the assumptions in the model (curvature versus ICS, vacuum gap versus slot gap) may shift the line up or down, but not by much. It seems a contrived coincidence that the conal emission mainly comes from pulsars that require some pair creation mechanism that is beyond the simple dipole model.

In light of our new model for weak pulsars, we propose a potential solution to both these puzzles that does not require non-dipolar field configuration. As discussed in Section 4.2,

when pair supply from the star is not enough, a vacuum gap is periodically opened around the separatrix up to the light cylinder. This gap, accelerating electrons back toward the star, can reach much higher potential drop than the maximum polar cap potential $\Phi_{\rm pc} \sim \mu_B \Omega^2/c^2$, approaching the vacuum potential drop $\Phi_0 \sim \mu_B \Omega/R_* c$. This makes pair creation possible even if the polar cap voltage is insufficient, but the pair creation activity will be confined to the return current, along a ring-like structure around the polar cap. This could in principle lead to the disappearance of the strong core radio component produced by pairs created at the center of the polar cap, and the appearance of a conal component near the edge of the polar cap due to the pairs created along the current sheet.

Pulsars with conal emission often also exhibit the "drifting subpulses" phenomenon (see, e.g., Rankin 1993). The timescale for these subpulse modulations is typically observed to be $P_3 \sim$ 2–15 period cycle^{-1}. These modulations were thought to be associated with drifting local pair discharge activity, or local "sparks" (e.g., Ruderman & Sutherland 1975). A potential alternative explanation could simply be that P_3 is the cycle presented in Section 4.2, and is regulated by the plasma flow between the stellar surface and the pair cloud near the light cylinder, especially if the period for the cyclic behavior scales with the pair multiplicity. In order to validate or disprove this hypothesis, 3D simulations in the similar parameter regime are likely needed.

6. Discussion

In this paper we presented a range of self-consistent solutions of the pulsar magnetosphere. We found that even when pair creation is restricted to be near the surface, weak pulsars can produce enough pairs to fill the magnetosphere and reach a near force-free state.

Depending on how easy it is to produce the pairs, these weak pulsars may settle down to a near-death state as reported in CB14, or stay in a highly variable state where pair creation and current flow are intermittent, or reach a near force-free state that is very similar to Type I pulsars. This should be compared with the range of solutions obtained by Cerutti et al. (2015) where pairs are supplied artificially from the stellar surface. What we found in this paper is that with copious pair supply near the star ($\eta \gtrsim 100$), our result with self-consistent pair creation is indeed very similar to the high pair injection rate solution reported by Cerutti et al. (2015): the magnetosphere is near force-free inside the light cylinder, and most of the Poynting flux dissipation happens outside the Y-point. However, in the low pair supply regime steady pair creation near the surface is not possible, and the magnetosphere has to go through episodes of opening and screening of the pair-accelerating gap, significantly increasing the dissipation inside the magnetosphere.

Compared with the results obtained by Gruzinov (2013), our low to intermediate pair supply ($\eta \lesssim 75$) solutions are somewhat similar in the sense that a large unscreened gap can exist in the outer magnetosphere. Especially in our $\eta = 25$, we do see a small amount of positrons flowing out near the separatrix, accelerated by the vacuum gap, and move across magnetic field lines. However, this solution has very low spindown power in the first place, and the pulsar activity is decreasing over time. Moreover, Gruzinov's solution did not contain a similar time-dependence, which we reported in Section 4.2. In the case of high pair supply, the magnetospheric differences between strong and weak pulsars virtually vanish, and we no longer observe such large vacuum gaps as our solutions become almost force-free.

In this paper we have used quite a simple model for pair creation, namely, whenever a particle hits a Lorentz factor threshold, it will immediately create an $e^{\pm}$ pair. In reality, the microphysics is much more complicated, as curvature photons will have an energy-dependent free path, which will allow particle acceleration beyond the threshold energy, and synchrotron cascade will further enhance the pair multiplicity by about an order of magnitude. Higher pair multiplicity from the cascade will definitely change the critical ratio $\gamma_{\rm pc}/\gamma_{\rm thr}$, potentially enabling the peculiar time-dependent pulsar solution when η is closer to unity. However, particularly when approaching the death line of $\gamma_{\rm pc} \sim \gamma_{\rm thr}$, finite photon free path depending on its energy and propagation direction will likely play a very important role in the global plasma supply and dynamics. This should be studied in detail in the future with a more sophisticated model for pair creation including the cross section for the pair production process derived from quantum electrodynamics, similar to what was developed by Grismayer et al. (2017).

We thank Andrei Beloborodov and Alexander Philippov for stimulating and helpful discussions. Some of the ideas in this paper were inspired by the discussions at the workshop "Magnetospheres of Neutron Stars and Black Holes" at Goddard Space Flight Center in 2019 June. The code *Aperture* used in this work can be found at https://github.com/fizban007/Aperture3.git. This work was supported by NASA grants NNX15AM30G and 80NSSC18K1099 and by the National Science Foundation under grant No. NSF PHY-1748958. We also gratefully acknowledge the support of NVIDIA Corporation with the donation of the Quadro P6000 GPU used for this research. F.C. is supported by the European Research Council (grant InPairs ERC-2015-AdG 695088) and the Fundação para a Ciência e a Tecnologia (FCT, grants PD/BD/114307/2016 and APPLAuSE PD/00505/2012). A.S. is supported by Simons Foundation (grant 267233).

ORCID iDs

Alexander Y. Chen https://orcid.org/0000-0002-4738-1168

References

Beloborodov, A. M. 2008, ApJL, 683, L41
Brambilla, G., Kalapotharakos, C., Timokhin, A. N., Harding, A. K., & Kazanas, D. 2018, ApJ, 858, 81
Cerutti, B., Philippov, A., Parfrey, K., & Spitkovsky, A. 2015, MNRAS, 448, 606
Cerutti, B., Philippov, A. A., & Spitkovsky, A. 2016, MNRAS, 457, 2401
Chen, A. Y. 2017, PhD thesis, Columbia Univ. doi:10.7916/D80V8R6G
Chen, A. Y., & Beloborodov, A. M. 2013, ApJ, 762, 76
Chen, A. Y., & Beloborodov, A. M. 2014, ApJL, 795, L22
Chen, K., & Ruderman, M. 1993, ApJ, 402, 264
Erber, T. 1966, RvMP, 38, 626
Grismayer, T., Vranic, M., Martins, J. L., Fonseca, R. A., & Silva, L. O. 2017, PhRvE, 95, 023210
Gruzinov, A. 2012, arXiv:1209.5121
Gruzinov, A. 2013, arXiv:1303.4094
Gruzinov, A. 2015, arXiv:1503.05158
Hibschman, J. A., & Arons, J. 2001, ApJ, 554, 624
Krause-Polstorff, J., & Michel, F. C. 1985, MNRAS, 213, 43P
Philippov, A. A., Cerutti, B., Tchekhovskoy, A., & Spitkovsky, A. 2015a, ApJL, 815, L19
Philippov, A. A., & Spitkovsky, A. 2014, ApJL, 785, L33

Philippov, A. A., & Spitkovsky, A. 2018, ApJ, 855, 94
Philippov, A. A., Spitkovsky, A., & Cerutti, B. 2015b, ApJL, 801, L19
Rankin, J. M. 1983, ApJ, 274, 333
Rankin, J. M. 1993, ApJ, 405, 285
Ruderman, M. A., & Sutherland, P. G. 1975, ApJ, 196, 51
Timokhin, A. N., & Arons, J. 2013, MNRAS, 429, 20
Timokhin, A. N., & Harding, A. K. 2019, ApJ, 871, 12
Weatherall, J. C., & Eilek, J. A. 1997, ApJ, 474, 407
Zhang, B., Harding, A. K., & Muslimov, A. G. 2000, ApJL, 531, L135